

ACHIEVING RGB-D LEVEL SEGMENTATION PERFORMANCE FROM A SINGLE TOF CAMERA

Pranav Sharma³, Jigyasa Singh Katrolia¹, Jason Rambach¹, Bruno Mirbach¹, Didier Stricker^{1,2}, Juergen Seiler³

¹German Research Center for Artificial Intelligence, Germany, ²RPTU Kaiserslautern, Germany, ³FAU Erlangen, Germany

ABSTRACT

Depth is a very important modality in computer vision, typically used as complementary information to RGB, provided by RGB-D cameras. In this work, we show that it is possible to obtain the same level of accuracy as RGB-D cameras on a semantic segmentation task using infrared (IR) and depth images from a single Time-of-Flight (ToF) camera. In order to fuse the IR and depth modalities of the ToF camera, we introduce a method utilizing depth-specific convolutions in a multi-task learning framework. In our evaluation on an in-car segmentation dataset, we demonstrate the competitiveness of our method against the more costly RGB-D approaches.

Index Terms— multi-modal image segmentation, depth image, infrared image

1. INTRODUCTION

The research field of semantic segmentation is dominated by RGB images. Only recently it shifted in the direction of RGB-D semantic segmentation [1, 2, 3, 4]. However, RGB images may not always be available due to practical, logistical and financial reasons. RGB-D cameras incur higher cost and more effort to calibrate the two cameras. Their larger package size often limits their place in real-world applications. Indeed, Time-of-Flight (ToF) depth cameras are often deployed without an accompanying RGB camera for applications like gesture control, in-car monitoring, industry automation and building management. Infrared images (IR) on the other hand are a by-product of ToF depth cameras (no additional sensor needed), but have not been explored sufficiently, specifically in combination with depth data [5, 6].

Infrared images from ToF cameras provide the magnitude of the modulated light reflected from the scene and contain shape and semantic features in a different spectral range [7]. Due to the similarities between RGB and IR images, it is natural to attempt to adapt existing RGB-D fusion approaches to combine IR and depth images. However, in most RGB-D methods depth information is only an accessory to the color information and is consumed by the same type of neural network layers despite their differences. Some recent works proposed depth-specific operations like depth-aware [2] and shape-aware [3] convolutions. We observe that both IR and

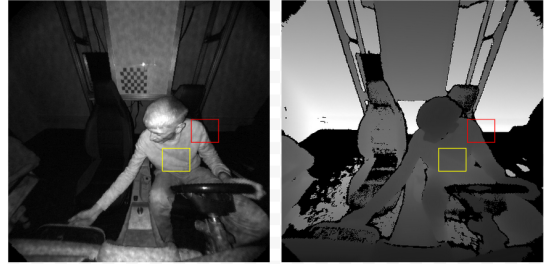


Fig. 1. Patch similarities of IR and Depth modalities of a ToF Camera.

depth outputs from a ToF camera are related in many ways and therefore these depth-specific operations can be applied to IR images as well. For example, the intensity of light reflected from an object decreases as distance to the object increases. Object surfaces closer to the camera will reflect more light implying that pixel intensities in an infrared image varies with the shape of that object. We can see this by comparing the same colored patches in Figure 1 and note how both image patches have same relative changes in pixel values. We use this observation to leverage the shape-aware convolution operation for both IR and depth images to learn more meaningful features from both modalities.

We aim to use the available modalities from a single ToF camera to achieve semantic segmentation performance comparable to RGB-D methods using an architecture that is tailored to IR-Depth (IR-D) input. We take inspiration from [3, 2] and design a depth-aware shape convolution operation that consumes IR-D input in a multi-task learning (MTL) architecture with depth filling as an auxiliary task. Our proposed method surpasses the baseline RGB-D based methods using only a ToF camera.

2. RELATED WORK

RGB-D Semantic Segmentation: A wide range of approaches have been proposed for incorporating the depth information in RGB-D semantic segmentation and can be broadly classified into three categories as outlined by [8]: (1) Using the depth channel as an additional input and performing fusion at different levels (early [9], feature-level [1] or

late [4] fusion); (2) Depth as supervision signal for auxiliary tasks such as depth estimation or completion [10] and (3) Depth-specific operations. Depth-Aware CNN [2] showed that object boundaries correlate with depth gradients and created *depth-aware convolution* and *depth-aware pooling* functions. ShapeConv [3] used a *shape convolution* kernel to ensure convolution kernels give consistent responses to object classes at different locations in the scene. [11] used depth information to adjust the neighbourhood size of a 3D convolution filter.

Depth and IR for Semantic Segmentation. Depth-only methods for semantic segmentation are typically applied to solve very specific tasks, like object manipulation via mechanical arm [12], hand segmentation or hand and object segmentation [13, 14]. Even fewer methods have explored the combination of IR and depth. [6] used IR to classify materials since the infrared response depends on the material of the object. [5] used IR image as an additional input channel for improving the depth predicted from a setup containing both stereo and ToF cameras

Multi-Task Learning (MTL). The survey by [15] describes many examples where simultaneous learning of two or more related tasks can boost the performance on either task. RGB-D segmentation is enhanced using auxiliary tasks like depth and surface normal prediction [16]. MTL methods typically employ a single encoder to learn features from the available input modalities and two separate task-specific decoders to perform prediction [16].

3. BACKGROUND AND NOTATION

3.1. ShapeConv: Shape-aware Convolutional Layer

In order to design convolutions that are invariant to different depth values (*base*) when the underlying relative difference in depth in a local patch (*shape*) remains same, ShapeConv [3] suggested decomposing an image patch $\mathbb{P} \in R^{K_h \times K_w \times C_{in}}$ into a *shape* component \mathbb{P}_s and a *base* component \mathbb{P}_b . These two components are operated on separately by a corresponding shape \mathbb{W}_S and base kernel \mathbb{W}_B before being passed to the standard convolutional kernel \mathbb{K} . Instead of decomposing the image patch, the convolutional kernel itself can be decomposed to the respective components as shown in equation (1). Here $m(\mathbb{K})$ refers to mean of the kernel.

$$\begin{aligned} \mathbb{K}_B &= m(\mathbb{K}) \\ \mathbb{K}_S &= \mathbb{K} - m(\mathbb{K}) \end{aligned} \quad (1)$$

Shape convolution is then written with *ShapeConv* as:

$$\begin{aligned} \mathbb{F} &= \text{ShapeConv}(\mathbb{K}, \mathbb{W}_B, \mathbb{W}_S, \mathbb{P}_i) \\ &= \text{Conv}(\mathbb{W}_B \diamond m(\mathbb{K}) + \mathbb{W}_S * (\mathbb{K} - m(\mathbb{K})), \mathbb{P}) \\ &= \text{Conv}(\mathbb{W}_B \diamond \mathbb{K}_B + \mathbb{W}_S * \mathbb{K}_S, \mathbb{P}) \\ &= \text{Conv}(\mathbf{K}_B + \mathbf{K}_S, \mathbb{P}) \\ &= \text{Conv}(\mathbf{K}_{BS}, \mathbb{P}) \end{aligned} \quad (2)$$

Here, \diamond and $*$ represents the base and shape product respectively. \mathbb{W}_B and \mathbb{W}_S are learnable weights corresponding to *base* and *shape* components respectively.

3.2. Depth-Aware CNN and Depth Similarity

In depth-aware convolution DCNN [2], pixels with similar depth values to the centre pixel are weighted more than other pixels. This property is named depth similarity. The depth similarity function $F_D(p_i, p_j)$ calculates the difference of depth values between two pixels p_i and p_j respectively.

$$F_D(p_i, p_j) = \exp(-\alpha |D(p_i) - D(p_j)|) \quad (3)$$

Depth-aware convolution is written with the depth similarity function F_D as:

$$y(p_0) = \sum_{p_n \in R} w(p_n) F_D(p_0, p_0 + p_n) x(p_0 + p_n) \quad (4)$$

In Equation (4), the depth similarity term (F_D) is introduced with the convolution operation. The convolved features are weighted by F_D . The parameter α weighs the influence of the depth similarity function F_D on the convolution operation.

4. METHOD

We propose a depth-aware shape convolution operation and use it in a multi-task learning network. Our primary task is semantic segmentation using concatenated infrared and depth images from a ToF camera and the auxiliary task is depth completion for missing pixels in raw depth images.

4.1. Depth-Aware Shape Convolution

We design a depth-aware shape convolution, where the shape kernel in ShapeConv is supplemented with the depth similarity measure F_D as computed in equation (3). Formally, this integration can be written in two steps. First the kernel is decomposed into *shape* and *base* kernel as shown in equation (2). After the calculation of the weights \mathbf{K}_{BS} , the term $w(p_n)$ in equation (4) is replaced with \mathbf{K}_{BS} calculated from shape kernel. In this way, kernel weights calculated using shape kernel are integrated with depth similarity of DCNN. Equation (3) can thus be rewritten for Depth-aware ShapeConv as:

$$y(p_0) = \sum_{p_n \in R} \mathbf{K}_{BS_n} F_D(p_0, p_0 + p_n) x(p_0 + p_n) \quad (5)$$

4.2. Infrared and Depth-Aware Multi-Task Network

We realize a hard parameter sharing-based multi-task network with semantic segmentation as the main task and depth-filling as the auxiliary task (Figure 2). We use ResNet-101 as the backbone feature extractor to encode features from concatenated infrared and depth (IR-D) images. The convolution

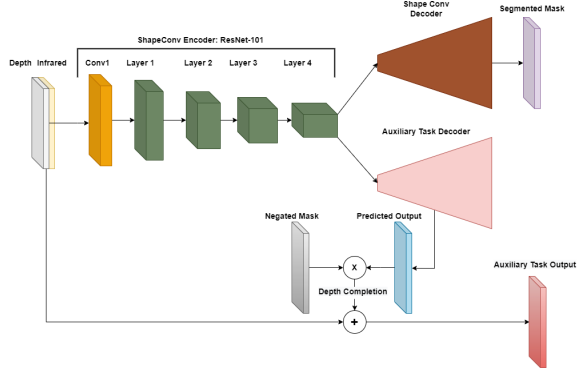


Fig. 2. MTL architecture for segmentation task and dense depth prediction using depth-aware shape convolutions.

layers in the ResNet encoder are replaced with depth-aware shape convolutions presented in section 4.1. The extracted features are passed to two task-specific decoders that generate final segmentation masks and depth values for missing pixels. For training the depth filling branch, the ground truth is prepared as described in section 5.1. We follow the training strategy from [17] and use predicted depth values only for missing pixels to calculate the error between ground truth and predicted depth. The dense depth map predicted by the network is then multiplied with the missing pixels mask (1 for missing pixels, 0 otherwise) to keep predicted depth values only for the pixels that are missing in raw image. The remaining values are then replaced by the corresponding depth values in input image.

5. EXPERIMENTS

5.1. Dataset

We evaluate our approach on the in-car cabin dataset TICaM [18] that provides RGB, depth and infrared images recorded with a single ToF camera and corresponding segmentation masks. Surprisingly we could not find any other dataset that provided segmentation masks for all three image modalities: RGB, depth and infrared. We used the real image-set with the suggested split of 4666 training images and 2012 test images for our experiments. Following [18] we combine different object classes into a single 'object' class to have 6 object classes in total. The RGB images have different resolution and FoV to depth and infrared images. To align the images, the RGB images are first mapped to the pinhole model of the depth images. Subsequently all the images are centre-cropped to size 230×418 . Normalization of the infrared image is implemented by first removing the outliers by calculating 99th percentile of the image and then scaling the image to the range of 0-255. To further enrich the information, histogram equalization and gamma filtering are applied to the normalized infrared image.

Ground-truth preparation. To train auxiliary task of dense depth prediction, filled depth images are required as ground truth. As TICaM dataset only provides depth images with holes, filled versions of these depth maps are artificially created in this work using "Colorization using Optimization" scheme [19]. The depth images are filled by enforcing similar depth values to the neighbouring pixels with similar intensities. The information on pixel intensities is provided by infrared images. During training, the error is calculated for the missing pixels following the training strategy of [17].

5.2. Baselines

We choose three existing methods for RGB-D segmentation and train them on both RGB-D and IR-D images to establish our baselines and better evaluate the difference between RGB-D and IR-D inputs. We choose FuseNet [1] since it is an established and well-tested network on many benchmark datasets for RGB-D segmentation, however it has not been tested yet on TICaM dataset. ShapeConv and Depth-aware CNN on the other hand are more recent methods that use novel convolution operations unlike FuseNet. FuseNet and Depth-aware CNN have VGG-16 backbone, while ShapeConv uses ResNet-101. All networks use SGD optimizer with a momentum of 0.9 and weight decay of 5×10^{-4} to update the weights. By default, Deeplab v3+ and ShapeConv use pre-trained weights while FuseNet and Depth-aware CNN are initialized using kaiming initialization [20]. For training with IR-D images we replicate infrared images to form 3-channel images and concatenate them with single channel depth images. We report pixel accuracy, class accuracy, mean Intersection-over-Union (IoU) and frequency weighted IoU (f.w.IoU) in Table 1 for all the baselines.

We can observe that the architectures that incorporate depth in an informed manner outperform FuseNet which simply concatenates depth with other modalities. Also, the combination of infrared and depth can be used instead of RGB-D input while achieving almost the same performance on segmentation but the disparity between the achieved performance is least when using depth-aware architectures with ShapeConv outperforming the other two baselines. We can see also from Figure 3 that ShapeConv with both 3-channel and 1-channel infrared images have similar mask predictions.

5.3. Experiments with Proposed Network

We progressively modify the ShapeConv architecture into a multi-task learning network for semantic segmentation on IR-D data. We first replace the 3-channel infrared input with 1-channel infrared image, and evaluate the resulting network (Table 2 row 1). Comparing this with Table 1 row four, we can notice slight improvement over most of the metrics while the number of model parameters decrease in the initial layers (Table 3 row one and two). We follow this by incorporating depth similarity into the ShapeConv as described in sec-

Table 1. Segmentation baselines for RGB-D and IR-D data. The input is always 4-channel with 3-channel RGB or infrared.

Input	Baselines	Pixel Acc.	Class Acc.	Mean IoU	f.w.IoU
RGB-D	ShapeConv [3]	97.86	81.25	77.39	95.92
	Depth-Aware CNN [2]	94.63	66.88	54.14	90.78
	FuseNet [1]	95.35	56.89	42.46	92.43
IR-D	ShapeConv [3]	97.75	81.31	74.61	95.76
	Depth-Aware CNN [2]	93.52	60.52	50.03	88.45
	FuseNet [1]	93.18	55.73	39.61	88.84

Table 2. Segmentation performance of suggested architectures. Input is always 2-channel concatenated IR-D image.

Method	Pixel Acc.	Class Acc.	Mean IoU	f.w.IoU
ShapeConv [3]	97.82	80.73	75.78	95.82
Ours DA-ShapeConv	97.57	85.08	78.39	95.42
Ours MTL-DA-ShapeConv	97.73	85.98	79.73	95.68

Table 3. Number of model parameters (in millions) and per image inference time (in milliseconds) for baselines and proposed MTL architecture. (Here, ch represents channels)

Method	Input	Params (million)	Time (ms)
ShapeConv [3]	4-ch	60.55	35.04
ShapeConv [3]	2-ch	60.54	32.20
Ours DA-ShapeConv	2-ch	60.54	37.12
Ours MTL-DA-ShapeConv	2-ch	78.12	37.16

tion 4.1 and name the realized method DA-ShapeConv (Depth Aware ShapeConv). We can note that combining both depth-aware and shape convolutions gives significant improvement on class accuracy as well as mean IoU. Finally, we train our proposed MTL network (MTL-DA-ShapeConv) and present the quantitative and qualitative results. We can see that the MTL architecture improve over the best performing RGB-D ShapeConv baseline from Table 2, with significant improvement in class accuracy and mean IoU. This shows using our MTL network, one can outperform state-of-the-art RGB-D methods using images provided by a single ToF camera.

6. CONCLUSION

We designed a network for IR-D segmentation that performs equally well as RGB-D segmentation so that inconvenient and expensive RGB-D cameras can be replaced with single Time-of-Flight (ToF) cameras. We showed that existing fusion approaches for RGB-D segmentation can be used with IR-D input if standard convolutions are replaced with depth-specific convolutions. We then presented a combination of depth-aware and shape-aware convolutions, and designed a

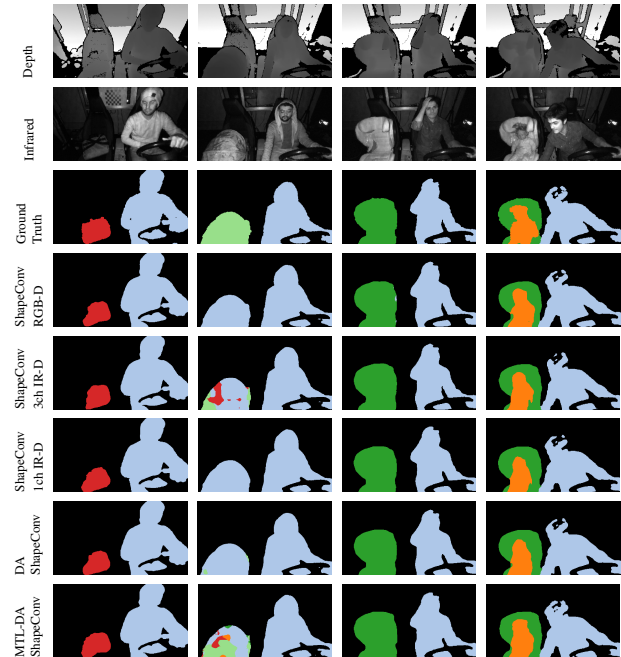


Fig. 3. Predictions from RGB-D and proposed I-D methods.

multi-task learning (MTL) architecture with this new convolution operation. We employ hard parameter sharing between our main and auxiliary tasks of segmentation and depth filling respectively. Through progressive modifications to the input, the convolution operation, and the network architecture we showed that we can outperform all baseline methods. We conclude that using images from a single ToF camera, it is possible to surpass RGB-D segmentation performance with our designed MTL architecture.

7. REFERENCES

- [1] Caner Hazirbas, Lingni Ma, Csaba Domokos, and Daniel Cremers, “Fusenet: Incorporating depth into semantic segmentation via fusion-based cnn architecture,” in *Asian Conference on Computer Vision, 2016*. Springer, 2017, pp. 213–228.
- [2] Weiyue Wang and Ulrich Neumann, “Depth-aware cnn

- for rgb-d segmentation,” in *European Conference on Computer Vision (ECCV)*, 2018, pp. 135–150.
- [3] Jinming Cao, Hanchao Leng, Dani Lischinski, Daniel Cohen-Or, Changhe Tu, and Yangyan Li, “Shapeconv: Shape-aware convolutional layer for indoor rgb-d semantic segmentation,” in *IEEE/CVF International Conference on Computer Vision (ICCV)*, 2021, pp. 7088–7097.
- [4] Yanhua Cheng, Rui Cai, Zhiwei Li, Xin Zhao, and Kaiqi Huang, “Locality-sensitive deconvolution networks with gated fusion for rgb-d indoor semantic segmentation,” in *IEEE Conference on Computer Vision and Pattern Recognition (CVPR)*, 2017, pp. 3029–3037.
- [5] Gianluca Agresti, Ludovico Minto, Giulio Marin, and Pietro Zanuttigh, “Deep learning for confidence information in stereo and tof data fusion,” in *IEEE International Conference on Computer Vision Workshops (CVPR-W)*, 2017, pp. 697–705.
- [6] Shuochen Su, Felix Heide, Robin Swanson, Jonathan Klein, Clara Callenberg, Matthias Hullin, and Wolfgang Heidrich, “Material classification using raw time-of-flight measurements,” in *IEEE Conference on Computer Vision and Pattern Recognition (CVPR)*, 2016, pp. 3503–3511.
- [7] Uwe Hahne, *Real-time depth imaging*, Ph.D. thesis, Berlin Institute of Technology, 2012.
- [8] Sami Barchid, José Mennesson, and Chaabane Djéraba, “Review on indoor rgb-d semantic segmentation with deep convolutional neural networks,” in *International Conference on Content-Based Multimedia Indexing (CBMI)*. IEEE, 2021, pp. 1–4.
- [9] Hangke Song, Zhi Liu, Huan Du, Guangling Sun, Olivier Le Meur, and Tongwei Ren, “Depth-aware salient object detection and segmentation via multiscale discriminative saliency fusion and bootstrap learning,” *IEEE Transactions on Image Processing*, vol. 26, no. 9, pp. 4204–4216, 2017.
- [10] Jianbo Jiao, Yunchao Wei, Zequn Jie, Honghui Shi, Rynson W.H. Lau, and Thomas S. Huang, “Geometry-aware distillation for indoor semantic segmentation,” in *IEEE Conference on Computer Vision and Pattern Recognition (CVPR)*, June 2019.
- [11] Yunlu Chen, Thomas Mensink, and Efstratios Gavves, “3D neighborhood convolution: learning depth-aware features for rgb-d and rgb semantic segmentation,” in *International Conference on 3D Vision (3DV)*. IEEE, 2019, pp. 173–182.
- [12] Mingkan Zhou, Wei Song, Linyong Shen, and Yanan Zhang, “Stacked objects segmentation based on depth image,” in *International Conference on Optical and Photonic Engineering (icOPEN)*. SPIE, 2018, vol. 10827, pp. 363–368.
- [13] Mohammad Rezaei, Farnaz Farahanipad, Alex Dillhoff, Ramez Elmasri, and Vassilis Athitsos, “Weakly-supervised hand part segmentation from depth images,” in *Pervasive Technologies Related to Assistive Environments*, 2021, pp. 218–225.
- [14] Guan Ming Lim, Prayook Jatesiktat, Christopher Wee Keong Kuah, and Wei Tech Ang, “Hand and object segmentation from depth image using fully convolutional network,” in *International Conference of the IEEE Engineering in Medicine and Biology Society (EMBC)*. IEEE, 2019, pp. 2082–2086.
- [15] Michael Crawshaw, “Multi-task learning with deep neural networks: A survey,” *arXiv preprint arXiv:2009.09796*, 2020.
- [16] Yufeng Wang, Yi-Hsuan Tsai, Wei-Chih Hung, Wenrui Ding, Shuo Liu, and Ming-Hsuan Yang, “Semi-supervised multi-task learning for semantics and depth,” in *IEEE/CVF Winter Conference on Applications of Computer Vision (WACV)*, 2022, pp. 2505–2514.
- [17] Junbo Mao, Jupeng Li, Feng Li, and Chengkai Wan, “Depth image inpainting via single depth features learning,” in *International Congress on Image and Signal Processing, BioMedical Engineering and Informatics (CISP-BMEI)*. IEEE, 2020, pp. 116–120.
- [18] Jigyasa Singh Katrolia, Ahmed El-Sherif, Hartmut Feld, Bruno Mirbach, Jason R. Rambach, and Didier Stricker, “Ticam: A time-of-flight in-car cabin monitoring dataset,” in *British Machine Vision Conference (BMVC)*, 2021, p. 277.
- [19] Anat Levin, Dani Lischinski, and Yair Weiss, “Colorization using optimization,” *ACM Transactions on Graphics*, vol. 23, 06 2004.
- [20] Kaiming He, Xiangyu Zhang, Shaoqing Ren, and Jian Sun, “Delving deep into rectifiers: Surpassing human-level performance on imagenet classification,” in *Proceedings of the IEEE international conference on computer vision*, 2015, pp. 1026–1034.